Design and Analysis of a Space Sextant for High Altitude Navigation

Howard A. Garcia* and William J. Owen*
Martin Marietta Aerospace, Denver, Colo.

This paper describes the results of a preliminary design and analysis of a new spacecraft navigation system which is designed to operate autonomously in Earth orbits. The sensor, known as the Space Sextant, in combination with an on-board computing system, will be capable of determining the spacecraft's position and attitude for any orbit in cislunar space with comparable accuracy. The Space Sextant is basically an angle measuring device employing two connected and independently servoed trackers which are capable of approximately 0.6 arc sec included angle measurement accuracy. An estimated navigation accuracy of about 800 ft is obtained by measuring angles between the moon's bright limb and the bright stars. An estimated attitude accuracy of about 0.4 arc sec is obtained by referring the measured star directions to two orthogonal, body-fixed reflecting surfaces.

Introduction

FUTURE space missions may involve a new species of Earth orbits that will carry an unmanned spacecraft to extremely high altitudes which, in some cases, may be a substantial fraction of the Earth-moon distance. Autonomy in operation for scientific satellites will help to reduce the work load of the associated ground support facilities. Autonomy in operation for military satellites will enhance the ability of these satellites to remain undetected for indefinite periods of time.

The spacecraft navigation system under development and described here will have the advantage of complete autonomy because it does not depend upon man-made radiations in any form, either active or passive. Moreover, because of the nature of the observables, i.e., the moon and the stars, the system accuracy is almost completely indifferent to orbit size, shape, and orientation within the Earth-moon domain.

I. Navigation Concept

The navigation system is conceptually simple and totally self-contained. Navigation is accomplished by means of making angular measurements between the bright limb of the moon and the brighter stars (visual magnitude <3.0). Reduction to the moon's center of figure (approximating the center of mass), including the compensation for asphericity and lunar terrain effects, is accomplished by the on-board software system. The essential data required to determine the spacecraft state are, therefore, the measured angle, the moon's stored ephemeris, a model of the lunar terrain and the precisely recorded time of measurement. Figure 1 illustrates the basic geometry of the system.

In principle, it may be shown that a measured angle between a star at virtually infinite distance and an object such as the moon at a finite distance, places the navigator somewhere on the surface of a cone with the cone apex at the position of the object and the cone axis in the direction of the star. A second measurement to another star and the same nearby object establishes a line of position (line OM in Fig. 2) which places the navigator somewhere along the intersection of the two cones (where the second ambiguous intersection is obviated by the navigator's approximate knowledge of his position). No further position information is possible solely on the basis of additional star measurements except for the inevitable refinement of the original line of position. However, because the spacecraft and the moon move relative to one another, new lines of position are continually obtained. Moreover, old lines of position are in effect projected forward in time in highly predictable manner by virtue of the dynamical laws that govern the motion of the spacecraft.

The principal difficulty with this concept is that convergence times are relatively long for this navigation mode, depending largely upon the mean altitude (period) of the satellite orbit. Because Air Force requirements insist upon short convergence times from the onset of navigation, possibly involving large state errors, we have invoked in our analysis similar measurements made on the Earth's bright limb. This establishes a second line of position, the intersection of which with the first obtains a complete position fix in as short a period of time as is necessary to complete these measurements, i.e., a few minutes. From an approximate initial position obtained in this manner, the navigation filter with additional moon measurements is able to refine the position and velocity states of their final steady-state accuracies in substantially less than on day of operation. These accuracies are on the order of 800 ft in position and 0.01 fps in velocity for a twelve hour orbit to about 0.09 fps in velocity for an eleven day orbit, the position accuracy being about the same for both orbits.

II. Space Sextant

Measurement Concept

The basic principle of angle measurement is illustrated in Fig. 3. Consider for the moment that each tracker is locked onto its respective target and that a very narrow window is rotating with the wheel at constant angular velocity. As the window passes through the optical axis of tracker A, the timing sensor A sees an impluse of light (T_1). As the window continues in its arc, it will pass through the optical axis of tracker B, at which time timing sensor B sees an impulse (T_2). The included angle is $\theta_1 = \omega\ (T_2 - T_1)$. As the window continues its arc, it will again pass through the optical axis of tracker A, at which instant the timing sensor A sees an impluse (T_3) producing $\theta_2 = \omega(T_3 - T_2)$. This angle is the complement of θ_1 and is subsequently complemented on transfer to the computer to provide a second measurement of the proper angle.

Figure 4 is a cross section of the space sextant showing the principal optical paths, the gimbal arrangement, wheel motor,

Presented as Paper 75-1073 at the AIAA Guidance and Control Conference, Boston, Mass., Aug. 20-22, 1975; submitted April 19, 1976; revision received Aug. 9, 1976. This research was supported in part by the Space and Missile Systems Organization, United States Air Force Systems Command.

Index categories: Earth Satellite Systems, Unmanned; Spacecraft Navigation, Guidance, and Flight-Path Control Systems.

*Staff Engineer.

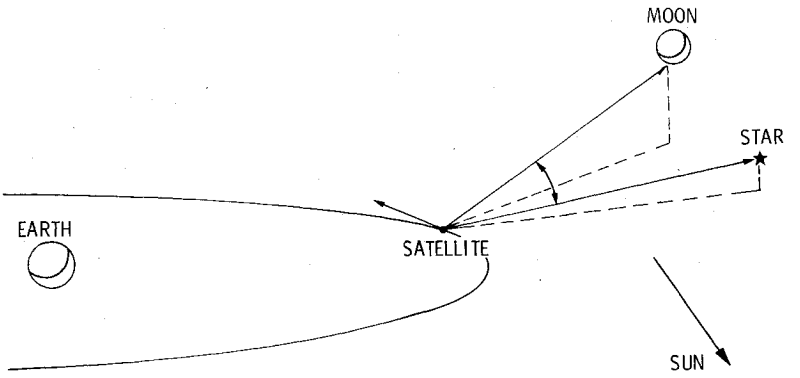

Fig. 1 Space Sextant navigation concept.

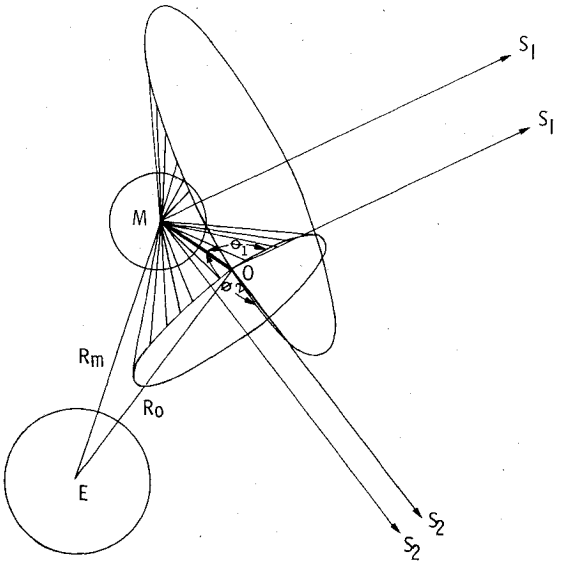

Fig. 2 Navigation principle using two-star measurements.

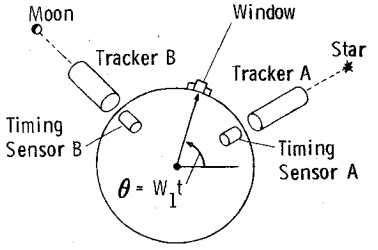

Fig. 3 Wheel angle measurement principle.

servo motor, and the photo detectors. As indicated the operation of each telescope is identical in all respects making it possible to track the moons's limb or a star with either telescope.

There are two optical paths in each telescope, one for tracking the celestial object, the other for generating the timing pulses. The tracking ray enters the telescope at 1) (both telescopes pointing downwards in the figure), reflects off of the primary objective mirror 2), the spherical secondary mirror 3), and finally impinges on the detector 4). This path is used to develop the necessary pointing error signals for the respective in-plane and cross-plane pointing servos.

The timing ray originates at an internal light source 5), emerges from a pinhole 6), and is collimated 7) before being split into two branches by the prism which diverts half of the energy into each telescope. The prism 8) is coaxial with the wheel 9) and turns with it. At one instant in each revolution of the wheel the timing ray is exactly parallel with one telescope axis and the opical path is completed to its Cassegranian focus 4) where the same detector is used to sense both the tracking ray and the timing ray. The time that this occurs depends upon the relative orientation of the telescope with respect to the case, and the time difference between pulses depends upon the relative orientation of the two telescopes. The timing pulse from each sensor is used to start and stop a digital counter that counts a precision clock. The corresponding binary number represents the properly scaled scalar angle between the telescopes' optical axis. The wheel speed is approximately 8 rps, yielding 16 measurements per second which are normalized to obtain one statistically averaged measurement to be used by the navigation filter.

An essential condition for accurate scalar angle measurement is that ω, the angular velocity of the wheel, be constant to a high degree. Our experience in the development of a velocity/acceleration control loop for the dual-spin gas-bearing reaction wheel indicated that this goal could be achieved. In that development program a specification of 10^{-5} ft-lb-s momentum resolution was placed on the control loop. A consequence of that particular requirement was that the instantaneous wheel velocity could not deviate from the theoretical velocity by more than 1 part in 10^{-6}. Motor cogging torques and bearing frictional torques were easily controlled by a wideband closed-loop servo.

The momentum control requirements of the dual-spin reaction wheel are virtually identical to the Space Sextant wheel speed control. In the Space Sextant, unwanted reaction torques are reduced to those caused by the wheel position pickoff only. These torques are very systematic and consist of a fundamental frequency caused by the radial runout of the pickoff, a second harmonic caused by the oblateness of the pickoff, and two other harmonics, 2^{11} and 2^{12}, of the fundamental frequency. The 2^{11} and 2^{12} harmonics do not cause any instantaneous position error since: 1) they are high frequency (20 and 40 kHz) and filtered (second- order) by the compensation of the control loop, and 2) second-order mechanical filtering is achieved by the spinning wheel. The particular pickoff device used in this development was an electro-optical disc manufactured by Teledyne-Gurley containing a reference mark and two tracks (a cos and sin track).

A phase-locked loop (Fig. 5) was employed for velocity/acceleration control of the momentum wheel. In this loop, a carrier frequency is modulated by the sin and cos tracks to allow a phase measurement of the instantaneous wheel position at a high sample rate. The carrier frequency term ω_2 appears in both inputs to the phase-lock logic, and its frequency instability does not affect the wheel velocity. The only consequence is its affect on the sample frequency, which is of no concern for extremely high sample rates. The sin-modulated carrier is phase-shifted 90°. This carrier, when summed with the cos-modulated track, reduces to a frequency consisting of the carrier plus that determined by the wheel angular velocity, multiplied by 2^{11}, i.e., a true suppressed carrier system. The resulting frequency is fed to a zero-crossing detector. The final output is a train of pulses that are phase-compared with a pulse train of a frequency that represents a commanded angular velocity.

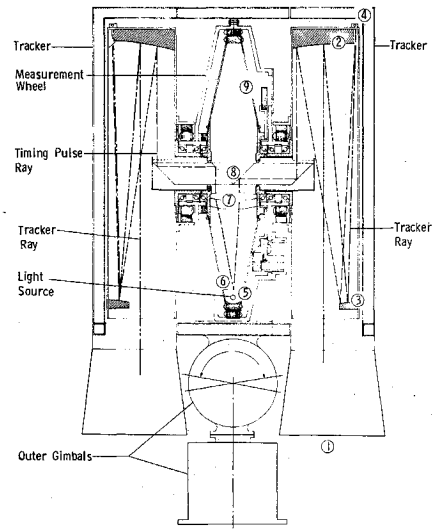

Fig. 4 Optical path.

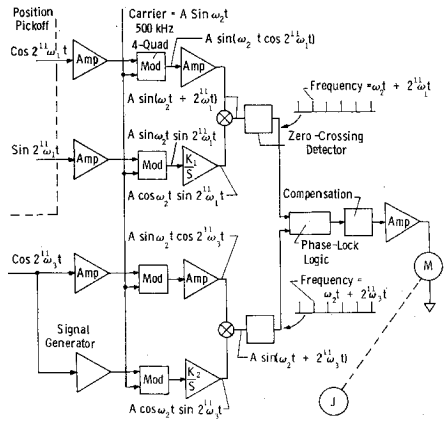

Fig. 5 Phase-locked speed control loop.

The phase error is fed to a high-gain motor drive circuit. The resulting overall loop gain is such that 30° of electrical phase error causes a saturation torque in the wheel drive motor. In a servoloop with such extremely high gain, the resulting loop errors are quite systematic and are caused solely by the peculiar frequency components that fall within the bandpass of the servoloop. These errors are caused by the physical characteristics of the pickoff disc and its mounting on the spin axis of the wheel (radial runout) and therefore have long-term repeatability. Simple techniques were developed during the study by which the errors can be reduced by one to two orders of magnitude, limiting the instantaneous position error of the wheel to less than 1 arc-sec, peak-to-peak. In the velocity control loop, bearing rolling friction and noise characteristics were studied as a function of preload. The effects of bearing noise on the control loop were negligible because of second-order mechanical filtering of the momentum wheel.

Detection, Acquisition, and Tracking

The high resolution of the sextant's measurements are attributable to the effective focal length of the optical system (1.5 m), the dimensions of the in-plane, fine track detectors (0.15 mm), and the technique of zero-crossing detection. The timing pulse is generated by the zero-crossing detection of the timing pulse ray as it crosses two dectectors whose output is differenced. One advantage of this type of detection is the accuracy that can be achieved, and another is its insensitivity to differences in detector responsivities.

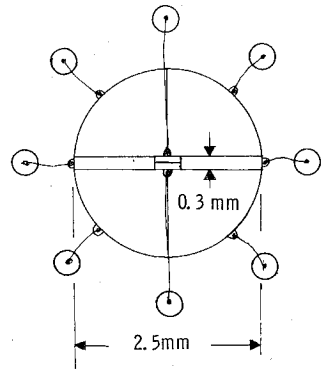

Fig. 6 Detector assembly.

The detectors are two-stage, four quadrant differential detection types, the first stage for acquisition and the second for precise tracking and timing pulse generation. The eight element detector for performing coarse acquisition for both moon and star, fine stellar tracking and fine lunar limb tracking is shown in Fig. 6. The individual elements are accessed electrically by small wires leading to eight terminals.

Coarse acquisition is accomplished by means of the four large quadrants with an effective angular radius at three arc-minutes. A signal sensed in any quadrant drives the servo system to position the target within the scope of the fine tracking sensors. The two long transverse sensors in combination with the narrow, split sensor at the center are used for tracking the bright limb. The split sensor, having an effective width (in the plane of measurement) of eighteen arc-seconds,is also used for fine stellar tracking.

In the illustration shown in Fig. 6 the plane of measurement is perpendicular to the paper and at right angles to the long transverse strip elements. Gimbal angles are computed with the approximate knowledge of the spacecraft attitude to orient one telescope on a star and the second on the bright limb in line with the center of the moon and the star. To be properly oriented for measurement the bright limb must illuminate both halves of the transverse element equally and produce a signal on the zero crossing detector. If the observed limb is not perpendicular to the plane of measurement the signals produced on the right and left sides will be mismatched, causing the outer and middle gimbal motors to reorient the plane of measurement until a balance is achieved. If the limb is too high or too low with respect to the center, a mismatch will be created in the top and lower halves, causing the inner gimbal motor to reorient the limb tracking telescope in the plane of measurement. Suitable logic will allow the measurement to be made on the bright limb whether the star is on the same or opposite sides of the moon's center. Terminator tracking is initially avoided by the commanded gimbal angles, and is ultimately rejected by the acquisition and fine tracking logic.

The preamplifier gains are individually adjusted for both detectors prior to each measurement to compensate for the varying brightness of the stars (up to +3.0 magnitude) and the varying brightness of the moon. A brightness index in appropriate units for each individual star is furnished to the sextant micro-computer along with the gimbal angles for each measurement. Similarly, a brightness index for the moon is computed as a function of phase and selenographic latitude.

A six arc-minute circular field of view was considered adequate for coarse acquisition in navigation where attitude reference was assumed to be furnished by an independent spacecraft system. A hardware modification to the sextant (not discussed here) to provide much larger coarse acquisition field of view is under development in the event the sextant is also used as an attitude reference sensor.

Servo Systems

The α (outer) and β (middle) gimbal servos are required to orient and maintain the measurement head in the plane of

measurement. They have two modes of operation. The first mode called "slew", is used in making the transition between stars. The command gimbals angles are computed by the navigation computer from a-priori knowledge of stars, time, lunar ephemeris, and attitude. The control loops are maintained in slew until star and limb acquisition signals are present. Upon acquisition, the gimbal loops switch to "track" and the gimbal servo pointing errors are derived from the fine sensors. The latter error signals are coordinate transformed to resolve the error signals into the proper components for the gimbal servo motors, which align the measurement head precisely into the plane of measurement.

The tracker servos are comparable to the gimbal servos, except that they have three modes of operation: 1) Slew – a mode used to drive the trackers in the measurement plane for acquisition. 2) Acquisition – a mode that is used to make a transition from coarse (wide field of view) sensors to fine (narrow-field-of-view) sensors. 3) Track – a mode that utitlizes pointing error signals derived from the in-plane fine sensor elements.

The next major servo loop is the wheel velocity servo. This is a phase-locked loop. The servos phase logic locks the feedback to a command frequency from the master oscillator. Errors in the feedback element are determined and compensated for in order to cause the wheel speed to be constant.

Systematic Error Compensation

To provide quantitative values and yield confidence in the preliminary design, a system model was developed that incorporated the dominant error sources. This model provided time solutions of the modeled servo state equations in conjunction with the support electronics, yielding time histories of sextant induced measurement errors. These errors are averaged over a one second measurement interval to produce "single measurement" error values. The standard deviation of a sample set was then calculated to yield the sextant's measuring capability of 0.56 arc sec (1 σ). Figure 7 shows the theoretical wheel position error with and without the error compensation system.

A "self-calibration" scheme for on-orbit sensor calibration has been worked out in theory. This technique is predicated on a fundamental design feature that permits either telescope to track a star (or the moon's limb). By measuring the angular separation between two known stars, the systematic tracker to tracker bias errors may be solved for and compensated for the onboard computer. The uncertainty in this calibration may be statistically averaged with the composite sensor noise to yield an overall random measurement error of approximately 0.6 arc-second.

Engineering Model and Laboratory Tests

An engineering model of the Space Sextant has been developed and tested to demonstrate the included angle measurement accuracy of the current design. This engineering model was developed primarily to demonstrate "proof of principle", and to obtain a laboratory verification of the in-plane measurement noise predicted by the theoretical model previously described. This first engineering model (Fig. 8), employing a single gimbal for in-plane measurement, contained several expedients made necessary by cost and schedule constraints, and consequently departed in many important respects from the ideal instrument design. However, despite these known deficiencies this suboptimal device was capable of 0.65 (1 α) arc-sec random noise, thus amply fulfilling its anticipated performance. A second engineering model now in development under Air Force sponsorship will incorporate the critical design features that should allow it to closely approximate the performance of the operational article with respect to measurement accuracy; moreover, this model will include additional refinements such as three gimbal servo actuators.

The laboratory demonstration for acquisition and tracking is also being carried out in two phases. Phase 1, just completed, has determined the measurement noise characteristics and in-plane tracking stability. This test utilized two star simulators for ideal target definition. A T-3 theodolite was used to measure the actual angle between the star simulators to an accuracy of ± 0.3 arc-sec. Figure 9 shows a schematic layout of this test setup.

Phase 2 will demonstrate the repeatability, noise, and bias of the sextant tracking a simulated lunar limb. The limb will

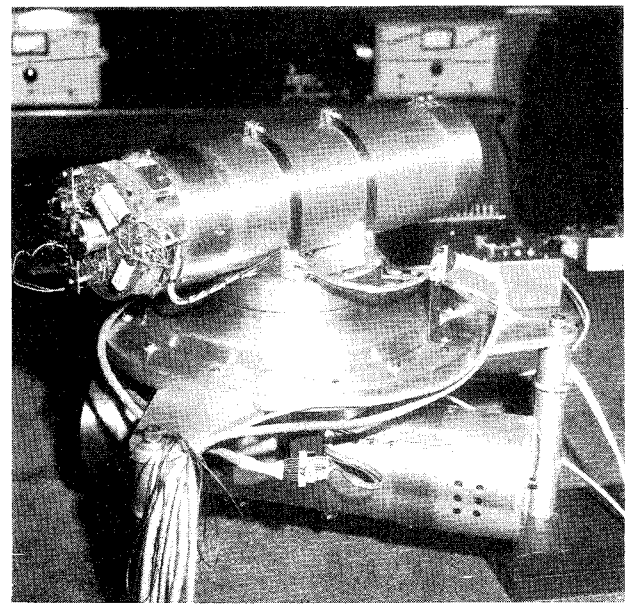

Fig. 8 Engineering test model.

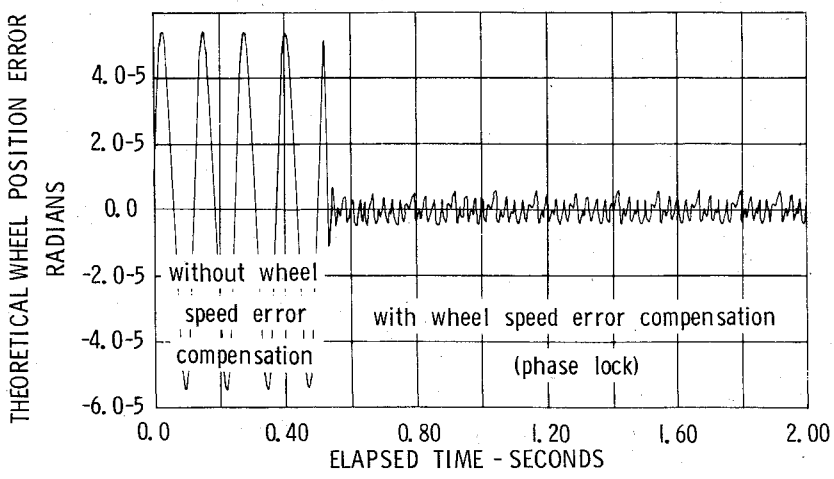

Fig. 7 Electronic systematic error compensation.

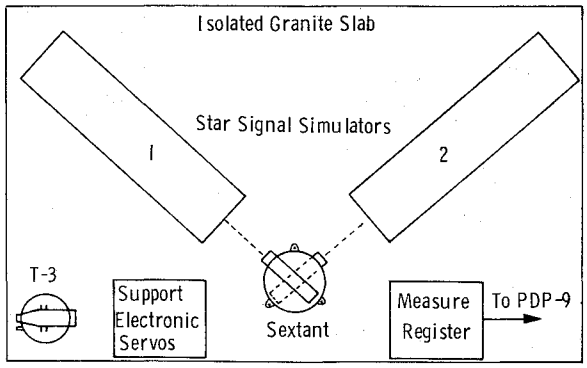

Fig. 9 Accuracy demonstration test setup.

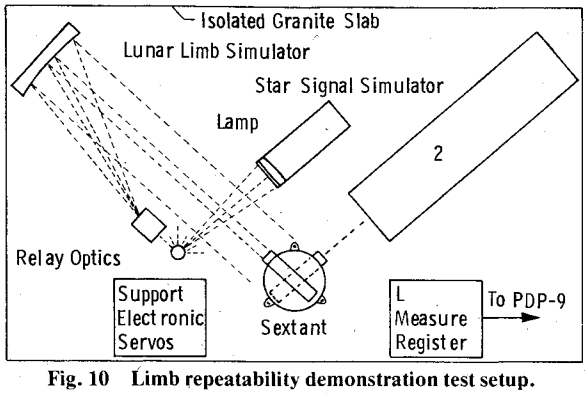

Fig. 10 Limb repeatability demonstration test setup.

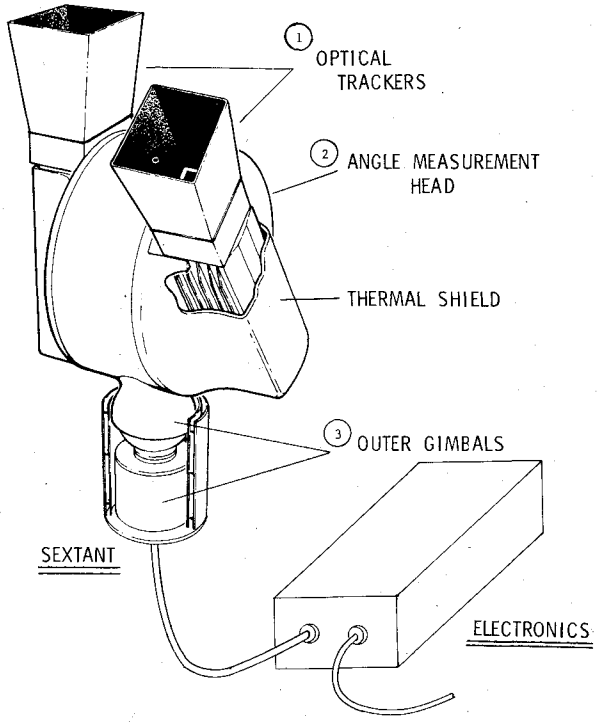

Fig. 11 Space Sextant angle measurement subsystem.

be simulated using a partially illuminated sphere of appropriate dimensions. Illumination will be provided with relay optics and an off-axis parabolic mirror shown in Fig. 10. Measurement accuracy and noise will be determined as a function of lunar phase angle and selenographic latitude. To study the effects of stellar type and brightness a 12-in. aperature star simulator will be used having variable magnitude and variable color temperature. In this phase, acquisition and tracking will be performed in three degrees of freedom.

Table 1 Angle measuring subsystem specifications

Telescopes		Detectors	
Focal length	: 1.5 m	Type	: silicon PIN
Free aperature	: 50. cm^2	Response	: 0.35 A/W
f/no., in-plane	: 15	Noise equiv. power	: 2×10^{-14} $W/\sqrt{HZ}$
f/no., cross-plane	: 30		
Type	: Dall-Kirkham	Current	: 2. p:a
			Thermal
Servos		Weight	Control
bandwidth	: 23 Hz	25 lb	Semi-passive
damping	: 0.7	Power	Hardening
noise equiv.	:1 arc-sec	25 W	JCS Spec
dynamic range	= ±8 arc-sec	Accuracy	Lifetime
		±0.6 arc-sec	5 years

Table 2 Ancillary subsystems specifications

Clock		Attitude reference unit	
short term stability	: 1.2×10^{-4}/day	accuracy: 10 arc-sec/axis (auxiliary attitude reference required where the Space Sextant is not used as its own attitude reference system)	
long term stability	: 3.4×10^{-9}		
uncompensated offset	: $1. \times 10^{-12}$		
Computer		Mass storage	
memory	: 16 K-32 bit words	stars[a]	:350 words
speed	: 15 K operations/sec	lunar ephemeris[b]	:1000 words/year
		lunar terrain[c]	:10 K words

[a] 70 stars, incl. brightness index, right ascension, proper motion (ra), declination, proper motion (decl).
[b] 20 Chebychev polynomial coefficient/axis/25 days.
[c] goal, projected on use of micro-grid storage format.

Preliminary Design Specifications

Figure 11 depicts the form of the Space Sextant resulting from the preliminary design phase. A provisional set of system specifications were also defined as a consequence of these studies. These specifications are presented in Tables 1 and 2 for the angle measuring subsystem and ancillary system components.

III. Navigation Performance Analysis

The principal outcome of the analytical investigation of the system performance was to demonstrate that the system will be capable of exceeding the Air Force's requirement for high altitude (above 5,000 n.mi.) by a substantial margin, both with regard to navigation accuracy as well as convergence times. To evaluate the overall navigation system's performance two parallel studies were launched. The first study being directed towards the determination of navigation sensitivities to various system errors, and the second study being dedicated to a rigorous estimation of navigation system accuracy by means of a nonlinear analysis.

Sensitivity Analysis

The sensitivy studies were carried out on five typical satellite orbits, and considered four categories of system errors, viz., sensor errors, initial spacecraft state errors, moon ephemeris errors, and lunar terrain errors. A relatively inexpensive statistical methodology was used in the sensitivity analysis whereby navigation errors, generated by a random process in the measurements (and other Gaussian system parameters), were averaged with respect to time along the or-

Table 3 Nominal budget for the four basic error sources

Parameter	Nominal error
Lunar ephemeris	607 ft (spherical)
Lunar terrain	1700 ft
Sensor noise	0.6 arc second
Initial state errors	Variable, depending on the orbit

Table 4 Test case orbits

Orbit tested	Period	Apogee n.mi.	Eccentricity	Inclination
A (Molniya)	12 hr	24,850	0.73	63.°4
B	24 hr	22,760	0.0	0.0
C	12 hr	14,350	0.0	63.°4
D	124 hr	68,000	0.0	90.0
E	272 hr	115,000	0.0	0.0

bit for one sample simulation using a "moving window" technique.

The principal advantage of using a simulation in performing sensitivity studies is that one may represent the trajectory errors statistically according to various schemes that are not possible in a covariance analysis. The sample statistics used here include two different methods for estimating the unbiased standard deviation, i.e., the square root second central moment, as well as a method for estimating the "biased" standard deviation, i.e., the origin moment. A comparison of these statistics provided a useful means for investigating systematic errors that may be present in the system. Furthermore, since the time averaging process tended to smooth output of the filter, it was possible to discern the time of convergence as well as estimate the steady state navigation error.

The main conclusions drawn fom the sensitivity study were that the system is essentially free of hidden system biases (such as the orbit, star/moon geometry, etc.) and that the system is not critically affected by any one error source or combination of errors where nominal error magnitudes are considered. The nominal error budget of the four basic error sources are shown in Table 3.

Lunar ephemeris errors are based upon an apparent position error of 0.1 arc sec at mean distance (207559 n. mi.) Lunar terrain errors are based on an expected randomness in the terrain height (the uncompensated part) of 0.28 arc sec, also reckoned at mean distance. Initial state errors in the form of correlated 6×6 covariance matrices varied from approximately 170,000 ft and 17 fps (1α rss) for the low orbit to approximately 17,000,000 ft and 10 fps (1σ rss) for the highest orbit tested. However, in addition to the above basically geometric errors, certain dynamic errors were imposed on the force models, i.e., small but sensible differences between the filter world (simulated orbit) and the real world (reference orbit). Process noise on the order of one 1 μ-g random acceleration was introduced in the simulations to enable the filter convergence to proceed in the presence of theses unmodeled forces. Similar procedures were also used in the Monte Carlo analysis to be described.

Perhaps one of the most important outcomes of the sensitivity analysis is the fact that the navigation system appears to be totally indifferent to orbit altitude, inclination and eccentricity. Figure 12 depicts the navigation error derived from star-moon measurements alone, following a limited period of mensuration, e.g., 7 hours for orbit A to 40 hours orbit E (see Table 4). Despite the large magnitude of the initial trajectory error and the wide variations of this errors for the different orbits, it is notable that close agreement was realized for orbits ranging in altitude from 400 n.mi. (orbit A periapsis) to 115,000 n.mi. (orbit E).

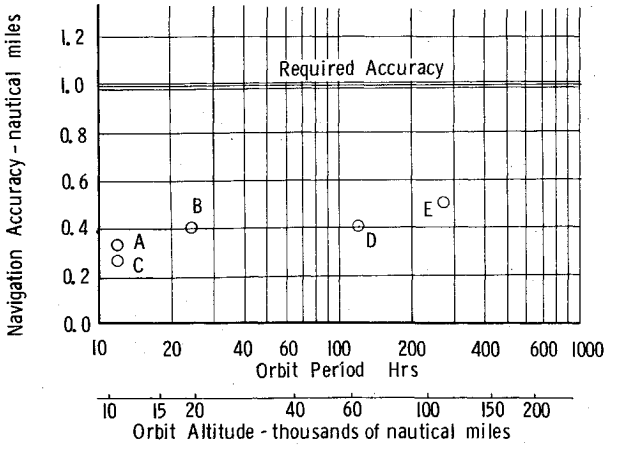

Fig. 12 Navigation accuracy: star-moon measurements.

These navigation errors, however, do not represent the ultimate accuracy of the system since the accuracy continues to improve with time up to perhaps a week or more of lunar observations, depending upon the period at the satellite orbit. Such long convergence times are not convenient for most Air Force missions; therefore, a means for reducing the time was considered highly desirable. The problem was solved by augmenting the star-moon measurements with star-Earth measurements. This strategem expedited the immediate reduction of large initial trajectory error and cut the time required to converge to 0.5 n.mi. from hours (and in some cases, days) to a matter of a few minutes. Thus, by circumventing the lengthy initial convergence process, it becomes possible to attain the ultimate system accuracy of about 800 ft on all orbits in substantially less time than one day of mensuration.

It is recognized, of course that the earth's limb provides a much poorer target for optical measurements than the moon's limb, and to register this effect of the error analysis an uncertainty of 6000 ft. (1σ) was applied to the geocentric radius after compensating only for the oblateness effect. Star-Earth navigation measurements are especially useful in two circumstances: 1) to reduce the large state errors at the onset of navigation; and 2) to suppress the growth of state errors during times when the moon is effectively occulted by the bright cone of light surrounding the sun. The ultimate accuracy of the navigation system, however, still rests on the lunar limb measurements, Earth limb measurements providing auxiliary support only during the special circumstances as noted.

Performance Analysis

A Monte Carlo analysis of the navigation system using two test orbits furnished the primary test bed for the definitive accuracy evaluation. The Monte Carlo method exposes the system to a rigorous, nonlinear analysis, providing the most complete measure by which system performance may be judged prior to the time that actual flight tests may begin.

Fifty-nine sample cases were run in compliance with the theory of order statistics in order to satisfy a 95% confidence level requirement for a 95% population coverage. The direct output of the Monte Carlo analysis included histograms and ensemble statistics of navigation errors for selected times along each orbit. Navigation errors for 67% population coverage (corresponding to the 1σ case), and for 95% population coverage (corresponding to the 2σ case) were obtained from the histogram data for each time point. These points were then connected, providing a continuous time history of navigation from the initial time to the converged steady state conditions.

The primary purpose of the Monte Carlo analysis was to verify the validity of the results on a comparatively few test cases of the less expensive sensitivity analyses which were performed on all of the orbits under investigation. The fact that

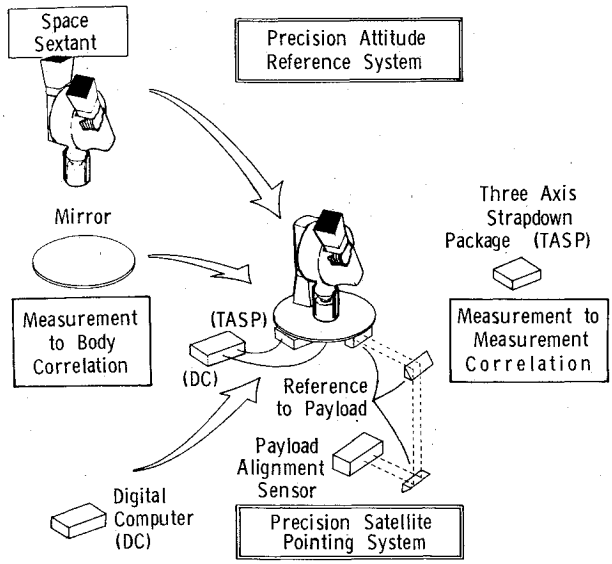

Fig. 13 Space Sextant attitude reference system.

the Mone Carlo analysis did indeed provide this corroboration in the presence of all known system errors confers a high degree of confidence to the basic conclusion derived in the study.

Space Sextant Attitude Reference System

Because of the inherent precision in angular measurement of the Space Sextant, it is highly advantageous to use the device as an attitude reference system in addition to being a navigation sensor. Three-axis angular orientation may be achieved by observing at least two stars with respect to two orthogonal reference planes rigidly attached to the spacecraft.

In principle, an angle may be measured between a star and one reference plane by orienting the optical axis of one telescope perpendicular to an optically flat reflecting surface (auto-collimation) while tracking the star with the second telescope. Using the Space Sextant in this mode, one may measure one angle directly with the full precision of the primary measurement head and a second angle with an azimuthal angle encoder in the base. A schematic of this procedure is illustrated in Fig. 13. Also shown is a conceptual optical train orienting the payload to the attitude sensor.

An alternative mode which exploits the full measurement precision of the sensor for two angles would be to erect a second auto-collimation device in the form of a vertical array of Porro prisms to reference the measured star to a second principal axis in the yaw plane. However, continuous attitude determination would be compromised by this method inasmuch as the second telescope would be required to slew periodically from one mirror to the other. Still a third alternative would be to use a second independent Space Sextant. Two sensors operating simultaneously would provide continuous attitude information.

Parametric investigations in attitude accuracy were conducted, analyzing the effects of various measurement errors, rate gyro stabilities, and measurement frequencies. The gyro drift magnitudes that were considered ranged from low performance (0.01 degrees hour) to high performance, space-qualified systems (0.001 degrees/hour). Commensurate scale factor errors were also considered for these graded-quality gyros. Measurement errors (white noise) of 1.0 and 2.0 arc-sec were imposed on the azimuthal angle encoder. These investigations indicated that the system is capable of satisfying Air Force requirements of 3.0 arc sec (1σrss), even for off-nominal conditions of up to three times the expected values of system errors.

A definitive performance analysis, applying the same rigorous Monte Carlo technique used in the navigation study, was used for the evaluation of the Space Sextant attitude reference system. The basis assumptions for this analysis were as follows: a) Random gyro drift of 0.001 degrees/hour/axis, b) Random measurement noise of 0.6 arc-sec, c) Initial attitude error of 6 degrees/axis, d) Measurement interval of 20 sec. The Monte Carlo analysis yielded rss'd attitude errors of 0.4 arc-sec for a 67% population coverage, and 0.7 arc-sec for the 95% population coverage.

IV. Conclusions

The Space Sextant concept for autonomous, high altitude navigation is predicated on the principle of position determination in space using precisely measured angles between the moon and stars. This concept has been demonstrated to be highly accurate for high altitude orbits by an extensive error analysis which considered all of the known significant contributing error sources in the system. A preliminary hardware design of the sensor and a first generation laboratory test model have shown that 0.6 arc-sec measurement accuracy is an achievable goal using present day technology. Owing to the basic angular nature of the measurements the sensor has a great potential of being developed into a precise attitude reference device in addition to its navigation functions. Current developmental effort is being directed towards the design of a dual-function sensor to be flown experimentally aboard an Air Force spacecraft in 1980.

References

[1]Garcia, H. A., "The Contribution of Onboard Optical Instrumentation to Deep Space Navigation," AAS/AIAA Astrodynamics Specialists Conference, Ft. Lauderdale, Fla., Aug. 1971.

[2]Garcia, H.A., "An Analysis of Recent Advances in Autonomous Navigation for Near Earth Applications," AIAA Paper 73-876, Key Biscayne, Fla., 1973.

[3]Hand, J.A., "Star/Horizon Measurements for Onboard Spacecraft Navigation," ION National Space Meeting on Space Navigation – Present and Future, Houston, Tex., April 1969.

[4]Kasper, J. P., "Orbit Estimation Using Manual Space Navigation Sensors," ION National Space Meeting on Space Navigation – Present and Future, Houston, Texas, April 1969.

[5]Lampkin, B. A., and Smith, D. W., "Sextant Sighting Measurements from Onboard the Gemini 12 Spacecraft," N69-14332, Issue 4, NASA Ames Research Center, Moffett Field, Calif.

[6]"Space Sextant High Altitude Navigation System (SS-HANS) Study," Phase O Final Rept., MCR-75-5 Vol. 1-6, Martin Marietta Aerospace, Denver, Colo.